REPRESENTING MATRIX CRACKS THROUGH DECOMPOSITION OF THE DEFORMATION GRADIENT TENSOR IN CONTINUUM DAMAGE MECHANICS METHODS

Frank A. Leone, Jr.[1]

[1]Structural Mechanics and Concepts Branch, NASA Langley Research Center
Hampton, VA, USA 23681
Email: frank.a.leone@nasa.gov, web page: http://www.nasa.gov/

Keywords: Continuum damage mechanics; progressive damage analysis; finite element method

ABSTRACT

A method is presented to represent the large-deformation kinematics of intraply matrix cracks and delaminations in continuum damage mechanics (CDM) constitutive material models. The method involves the additive decomposition of the deformation gradient tensor into 'crack' and 'bulk material' components. The response of the intact bulk material is represented by a reduced deformation gradient tensor, and the opening of an embedded cohesive interface is represented by a normalized cohesive displacement-jump vector. The rotation of the embedded interface is tracked as the material deforms and as the crack opens. The distribution of the total local deformation between the bulk material and the cohesive interface components is determined by minimizing the difference between the cohesive stress and the bulk material stress projected onto the cohesive interface.

The improvements to the accuracy of CDM models that incorporate the presented method over existing approaches are demonstrated for a single element subjected to simple shear deformation and for a finite element model of a unidirectional open-hole tension specimen. The material model is implemented as a VUMAT user subroutine for the Abaqus/Explicit finite element software. The presented deformation gradient decomposition method reduces the artificial load transfer across matrix cracks subjected to large shearing deformations, and avoids the spurious secondary failure modes that often occur in analyses based on conventional progressive damage models.

1 INTRODUCTION

The National Aeronautics and Space Administration (NASA) Advanced Composites Project (ACP) has the goal to reduce current 5–10 year product development and certification timelines by 30 percent for composite material aerospace applications. The first technical challenge of ACP involves the assessment and improvement of computational tools capable of predicting the strength and life of composite aerospace structures. A wide range of computational tools exist for the modeling of progressive damage in composite materials, including cohesive zone modeling, continuum damage mechanics, peridynamics, the extended finite element method, etc. In continuum damage mechanics (CDM) models, the presence of a crack is accounted for by modifying select terms of the material stiffness tensor $\boldsymbol{C}$. The terms of the damaged material stiffness tensor $\boldsymbol{C^d}$ are set so that the stress $\boldsymbol{\sigma}$ calculated from the current strain $\boldsymbol{\varepsilon}$ accounts for the opening of the crack without explicitly modeling the crack itself (i.e., without changing the original mesh or introducing additional degrees of freedom to the model):

$$\boldsymbol{\sigma} = \boldsymbol{C^d} : \boldsymbol{\varepsilon} \tag{1}$$

The terms of the material stiffness tensor that are modified are often selected based on the assumption that crack normals are aligned with the principal material directions, e.g., softening the fiber-direction Young's modulus for fiber failure, or softening the matrix-direction Young's modulus and shear modulus for matrix failure. Several such ply-level, strain-based CDM models have been developed for fiber-reinforced materials with varying degrees of sophistication (e.g., [1–4]) and the models generally

perform well for representing the formation and development of damage, especially when applied in cases where the loading is primarily planar and failure is quasi-brittle.

Camanho et al. [5] developed a three-dimensional CDM material model that embeds a cohesive interface in a continuum to represent a matrix crack. The use of a cohesive interface to represent matrix damage allows for consistent intraply and interply mixed-mode matrix damage predictions and better represents the kinematics of a softened interface that is not necessarily aligned with the principal material directions. The orientation of the cohesive interface within the material is defined based on the predictions of a three-dimensional matrix failure criterion. Camanho's model is a smeared-crack approach that utilizes additive strain decomposition to separate the strain tensor supplied by the finite element (FE) solver into linear elastic and cracking strain components:

$$\boldsymbol{\varepsilon} = \boldsymbol{\varepsilon}_{\mathrm{el}} + \boldsymbol{\varepsilon}_{\mathrm{cr}} \tag{2}$$

where $\boldsymbol{\varepsilon}_{\mathrm{el}}$ represents the linear elastic deformation of the bulk material and $\boldsymbol{\varepsilon}_{\mathrm{cr}}$ represents the embedded cohesive displacement-jump. The distribution between the elastic and cracking strain components is determined by solving for the cohesive displacement-jump vector that minimizes the difference between the cohesive stress vector and the bulk material stress tensor projected onto the cohesive interface. The Camanho model is implemented as a VUMAT user material subroutine for use with three-dimensional solid elements in Abaqus/Explicit [6]. Model results were shown to correlate well with experimental load-displacement results for unidirectional off-axis compression, laminated center-cracked tension, and laminated open-hole tension specimens.

However, CDM material models based on strain measures suffer from inherent difficulties regarding the definition of the orientation of a crack with respect to the orientation of a continuum for problems involving large shear deformation. In geometrically nonlinear models, elements are formulated in the current configuration using current nodal positions, and the strain $\boldsymbol{\varepsilon}$ is derived from the current configuration of the material [6]. The use of the FE solver-supplied strain as the input to CDM material models in geometrically nonlinear models can cause the current crack orientation to be erroneously defined, with the magnitude of the error scaling up with shear deformation. Consider a two-dimensional continuum that contains a crack with a normal in the reference 2-direction. When subjected to simple shear deformation, the orientation of the continuum rotates. If the orientation of an open crack is defined in terms of the FE solver-supplied strains in the current configuration, the orientation of the crack normal also rotates. For a cracked continuum subjected to simple shear, however, the orientations of the bulk material and the crack should not rotate. An incorrectly defined matrix crack orientation can cause load transfer across matrix cracks and the prediction of spurious secondary failure mechanisms (e.g., fiber failure). In order to address these issues, CDM material models must better account for the kinematics of a cracked continuum under geometrically nonlinear conditions.

As in the smeared-crack CDM material model of Camanho et al. [5], the continuum-decohesive finite element (CDFE) of Prabhakar and Waas [7] utilizes an embedded cohesive law to represent the formation and growth of intraply cracks in fiber-reinforced materials. The CDFE method is a finite element formulation that involves applying the principle of virtual work to a cracked continuum, deriving an enriched set of displacements for real and internal dummy nodes, and generating an equivalent element stiffness for the cracked element through static condensation. The CDFE method has been implemented as a two-dimensional triangular element for use with an in-house code at the University of Michigan. Results of open-hole tension specimen models with various fiber orientations were solved, yielding good correlation with experimental strain and displacement fields measured by digital image correlation.

Finite element techniques that are specially developed for modeling cracks within solid materials, such as the extended finite element method (e.g., [8–10]) and the CDFE method [7], do not exhibit the geometrically nonlinear crack orientation issues of conventional strain-based CDM methods. However, the implementation of these specialized finite elements for use with commercial finite element solvers is difficult and precludes the use of existing finite element libraries. To take advantage of all of the

existing built-in capabilities of commercial FE programs, it is desirable to use constitutive material models to model damage, while achieving a predictive capability similar to those of specialized finite elements.

The goal of this paper is to present an improved approach for representing the kinematics of the formation, opening, and closure of matrix cracks in CDM material models for fiber-reinforced materials. The present method, which was originally outlined in reference [11] and detailed in reference [12], is an extension of the smeared-crack CDM material model of Camanho et al. [5] with improved predictive capability for geometrically nonlinear problems, especially in the presence of large shear deformations. In section 2 of this paper, the details of the deformation gradient decomposition (DGD) method are presented. In section 3, finite element model results for two case studies are presented and discussed with a comparison of results generated with a conventional strain-based CDM material model and with a CDM material model based on the DGD method.

2 DEFORMATION GRADIENT DECOMPOSITION CDM METHOD

The DGD method is based on the separation of the deformation gradient tensor $\boldsymbol{F}$ into two parts by additive decomposition, in a manner analogous to the additive strain decomposition of the smeared-crack model defined by equation (2). The two decomposed parts of $\boldsymbol{F}$ are (*i*) the deformation gradient tensor $\boldsymbol{F}_{\mathrm{B}}$, which represents the bulk material deformation, and (*ii*) the cohesive displacement-jump vector $\boldsymbol{\delta}$, which represents the deformation of an embedded cohesive crack. The derivation of the presented method is carried out at the constitutive material level so as to be compatible with any commercial finite element code with user-defined material subroutines. The presented method is herein presented in the context of being implemented as a VUMAT user material subroutine for use with three-dimensional solid elements in Abaqus/Explicit.

In section 2.1, the coordinate systems for the continuum, the bulk material, and the embedded cohesive crack are defined in the reference and current configurations. In section 2.2, the decomposition of the deformation gradient tensor is performed so as to provide consistent definitions for the bulk material and cohesive crack deformations. In section 2.3, local equilibrium is established between the bulk material and cohesive crack components, which allows the bulk material strain and stress to be calculated and the cohesive damage variable to be determined.

2.1 Bulk Material and Crack Coordinate Systems

A rectangular cuboidal continuum of fiber-reinforced material with the fiber direction initially aligned with the reference x_1-direction is considered. The undeformed continuum may contain a matrix crack with a crack normal $\hat{\boldsymbol{e}}_{\mathrm{N}}$ oriented at an angle α from the x_2-direction in the x_2–x_3 plane, as shown in Figure 1. The angle α is defined in the reference configuration and does not change once determined. The angle α is dependent on the local stress state and can be determined by using a failure criterion for fiber-reinforced materials that accounts for the stress state on the angle of the fracture plane (e.g., [13, 14]). For the present method, α may take on values from $-\tan^{-1}(l_2/l_3)$ to $\pi - \tan^{-1}(l_2/l_3)$.

The initial, undeformed reference configuration of the continuum is described by $\boldsymbol{X}_{\mathrm{R}}$. The three columns of $\boldsymbol{X}_{\mathrm{R}}$ are orthogonal vectors designated $\boldsymbol{X}_{\mathrm{R}}^{(1)}$, $\boldsymbol{X}_{\mathrm{R}}^{(2)}$, and $\boldsymbol{X}_{\mathrm{R}}^{(3)}$, with lengths equal to the undeformed dimensions of the continuum, l_1, l_2, and l_3, respectively, such that:

$$\boldsymbol{X}_{\mathrm{R}} = \begin{bmatrix} l_1 & 0 & 0 \\ 0 & l_2 & 0 \\ 0 & 0 & l_3 \end{bmatrix} \tag{3}$$

The current configuration of the continuum, $\boldsymbol{x}$, is a function of $\boldsymbol{X}_{\mathrm{R}}$ and the deformation gradient tensor $\boldsymbol{F}$:

$$\boldsymbol{x} = \boldsymbol{F}\boldsymbol{X}_{\mathrm{R}} \tag{4}$$

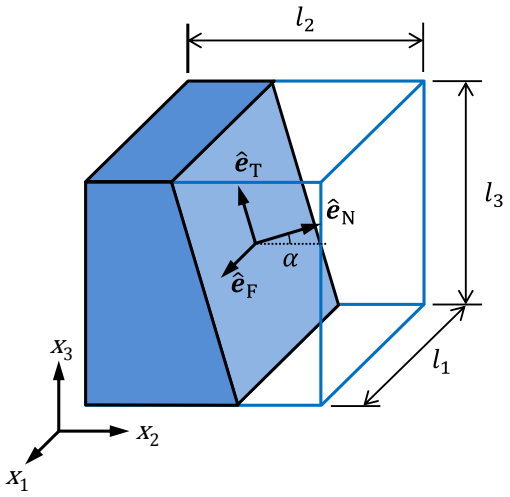

Figure 1: Schematic showing the orientation of the crack and dimensions of the continuum in the reference configuration.

The deformation gradient tensor $\boldsymbol{F}$ maps the coordinates defined in the reference configuration to their relative locations in the current configuration. $\boldsymbol{F}$ is easily computed from nodal displacements and is a known quantity that is generally provided by a finite element solver as an input for user-defined material models.

The reference configuration of the bulk material is equal to the reference configuration of the continuum. The current configuration of the bulk material, $\boldsymbol{x}_{\mathrm{B}}$, is a function of $\boldsymbol{X}_{\mathrm{R}}$ and bulk material deformation gradient tensor $\boldsymbol{F}_{\mathrm{B}}$:

$$\boldsymbol{x}_{\mathrm{B}} = \boldsymbol{F}_{\mathrm{B}}\boldsymbol{X}_{\mathrm{R}} \tag{5}$$

Prior to the initiation of damage, $\boldsymbol{F}_{\mathrm{B}}$ and $\boldsymbol{F}$ are equal. The method for solving for $\boldsymbol{F}_{\mathrm{B}}$ after the initiation of damage is presented in sections 2.2 and 2.3.

The orientation of the crack within the continuum can be described in terms of orthogonal unit vectors in the fiber, crack-normal, and transverse directions, $\hat{\boldsymbol{e}}_{\mathrm{F}}$, $\hat{\boldsymbol{e}}_{\mathrm{N}}$, and $\hat{\boldsymbol{e}}_{\mathrm{T}}$, respectively, as shown in Figure 1. These three unit vectors form the basis of the coordinate system $\boldsymbol{R}_{\mathrm{cr}}$:

$$\boldsymbol{R}_{\mathrm{cr}} = [\hat{\boldsymbol{e}}_{\mathrm{F}} \quad \hat{\boldsymbol{e}}_{\mathrm{N}} \quad \hat{\boldsymbol{e}}_{\mathrm{T}}] \tag{6}$$

In the reference configuration, the basis vectors of $\boldsymbol{R}_{\mathrm{cr}}$ depend only on α. In the current configuration, however, the deformation of the bulk material must be considered. For cases in which the crack is open, $\boldsymbol{R}_{\mathrm{cr}}$ is a function of $\boldsymbol{F}_{\mathrm{B}}$ and α:

$$\boldsymbol{e}_{\mathrm{F}} = \boldsymbol{F}_{\mathrm{B}}\begin{bmatrix}1\\0\\0\end{bmatrix} \tag{7a}$$

$$\boldsymbol{e}_{\mathrm{N}} = \boldsymbol{F}_{\mathbf{B}}^{-\mathrm{T}}\begin{bmatrix}0\\\cos\alpha\\\sin\alpha\end{bmatrix} \tag{7b}$$

$$\boldsymbol{e}_{\mathrm{T}} = \boldsymbol{e}_{\mathrm{F}} \times \boldsymbol{e}_{\mathrm{N}} \tag{7c}$$

where $\boldsymbol{e}_{\mathrm{F}}$, $\boldsymbol{e}_{\mathrm{N}}$, and $\boldsymbol{e}_{\mathrm{T}}$ are the non-normalized basis vectors of $\boldsymbol{R}_{\mathrm{cr}}$.

2.2 Decomposition of the Deformation Gradient Tensor

The bulk material deformation gradient tensor $\boldsymbol{F}_{\mathrm{B}}$ can be derived as a function of $\boldsymbol{F}$ and $\boldsymbol{\delta}$. Once a converged solution for $\boldsymbol{F}_{\mathrm{B}}$ is found, the stress and strain of the bulk material can be defined for any arbitrary deformation and any arbitrary angle α.

A schematic relationship is shown in Figure 2 between the deformation of the continuum ($\boldsymbol{x}$) and the deformations of its bulk material ($\boldsymbol{x}_{\mathrm{B}}$) and cohesive crack ($\boldsymbol{\delta}$) components in the x_1–x_2 plane for $\alpha = 0°$. In the figure, the crack is shown as being located along the top surface of the continuum, for clarity. However, the exact location of the crack within the continuum is ambiguous in CDM methods. As a result, it is necessary to make an assumption regarding the path of the crack through the continuum. In the present model, it is assumed that the crack crosses the continuum so as to intersect opposite pairs of surfaces of the continuum, i.e., the crack plane always intersects the surfaces whose normals are aligned with the x_1-direction in the reference configuration, and it intersects the surfaces whose normals are aligned with either the x_2- or x_3-directions in the reference configuration.

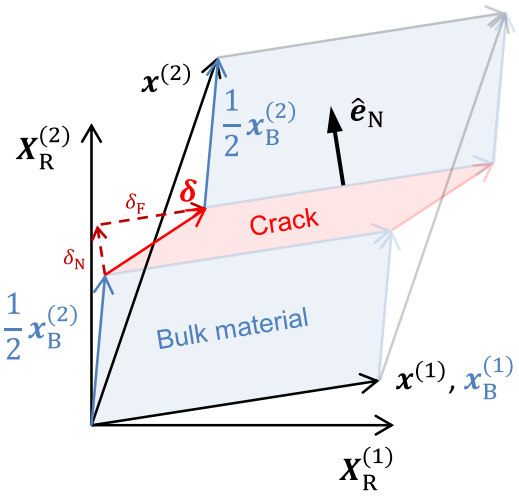

Figure 2: Decomposition of x_2-direction deformation for a partially opened crack with a crack normal $\hat{\boldsymbol{e}}_{\mathbf{N}}$ oriented at $\alpha = 0°$.

The first column of $\boldsymbol{F}_{\mathrm{B}}$ can be obtained from $\boldsymbol{F}$ by considering that the fiber-direction deformation does not depend on the presence, opening, or orientation of any matrix cracks. Because the crack-normal direction is always normal to the fiber-direction, the current configurations of $\boldsymbol{X}_{\mathrm{R}}^{(1)}$ calculated using $\boldsymbol{F}$ and $\boldsymbol{F}_{\mathrm{B}}$, $\boldsymbol{x}^{(1)}$ and $\boldsymbol{x}_{\mathrm{B}}^{(1)}$, respectively, are always equal:

$$\boldsymbol{x}^{(1)} = \boldsymbol{x}_{\mathrm{B}}^{(1)} \tag{8a}$$

$$\boldsymbol{F}\boldsymbol{X}_{\mathrm{R}}^{(1)} = \boldsymbol{F}_{\mathrm{B}}\boldsymbol{X}_{\mathrm{R}}^{(1)} \tag{8b}$$

Because only the first component of $\boldsymbol{X}_{\mathrm{R}}^{(1)}$ is nonzero, equation (8b) yields:

$$\boldsymbol{F}_{\mathrm{B}}{}^{(1)} = \boldsymbol{F}^{(1)} \tag{8c}$$

where $\boldsymbol{F}^{(1)}$ is the first column of $\boldsymbol{F}$ and $\boldsymbol{F}_{\mathrm{B}}{}^{(1)}$ is the first column of $\boldsymbol{F}_{\mathrm{B}}$.

For the crack shown in Figure 2, $\boldsymbol{X}_{\mathrm{R}}^{(2)}$ is intersected by the crack plane. As a result, the current configuration $\boldsymbol{x}^{(2)}$ is equal to the vector sum of the bulk material response $\boldsymbol{x}_{\mathrm{B}}^{(2)}$ and the cohesive displacement-jump vector $\boldsymbol{\delta}$ transformed into the reference configuration:

$$\boldsymbol{x}^{(2)} = \boldsymbol{x}_{\mathrm{B}}^{(2)} + \boldsymbol{R}_{\mathrm{cr}}\boldsymbol{\delta} \tag{9a}$$

$$\boldsymbol{F}\boldsymbol{X}_{\mathrm{R}}^{(2)} = \boldsymbol{F}_{\mathrm{B}}\boldsymbol{X}_{\mathrm{R}}^{(2)} + \boldsymbol{R}_{\mathrm{cr}}\boldsymbol{\delta} \tag{9b}$$

Because only the second component of $\boldsymbol{X}_{\mathrm{R}}^{(2)}$ is nonzero, equation (9b) yields:

$$\boldsymbol{F}_{\mathrm{B}}^{(2)} = \boldsymbol{F}^{(2)} - \frac{1}{l_2}\boldsymbol{R}_{\mathrm{cr}}\boldsymbol{\delta} \tag{9c}$$

where $\boldsymbol{F}^{(2)}$ is the second column of $\boldsymbol{F}$ and $\boldsymbol{F}_{\mathrm{B}}{}^{(2)}$ is the second column of $\boldsymbol{F}_{\mathrm{B}}$.

For the crack shown in Figure 2, $\boldsymbol{X}_{\mathrm{R}}^{(3)}$ is not intersected by the crack. As a result, $\boldsymbol{F}_{\mathrm{B}}{}^{(3)}$ can be derived using logic similar to the derivation of $\boldsymbol{F}_{\mathrm{B}}{}^{(1)}$, yielding:

$$\boldsymbol{F}_{\mathrm{B}}{}^{(3)} = \boldsymbol{F}^{(3)} \tag{10}$$

where $\boldsymbol{F}^{(3)}$ is the third column of $\boldsymbol{F}$ and $\boldsymbol{F}_{\mathrm{B}}{}^{(3)}$ is the third column of $\boldsymbol{F}_{\mathrm{B}}$. For cases in which the crack intersects $\boldsymbol{X}_{\mathrm{R}}^{(3)}$ instead of $\boldsymbol{X}_{\mathrm{R}}^{(2)}$, the derivations for the second and third columns of $\boldsymbol{F}_{\mathrm{B}}$ are swapped.

In order to write a generalized equation for $\boldsymbol{F}_{\mathrm{B}}$, it is necessary to account for whether the crack plane intersects $\boldsymbol{X}_{\mathrm{R}}^{(2)}$ or $\boldsymbol{X}_{\mathrm{R}}^{(3)}$, which depends on α, l_2, and l_3. The integer q can be used to define whether the crack intersects $\boldsymbol{X}_{\mathrm{R}}^{(2)}$ or $\boldsymbol{X}_{\mathrm{R}}^{(3)}$. When $\alpha \leq \tan^{-1}(l_2/l_3)$, the crack plane intersects $\boldsymbol{X}_{\mathrm{R}}^{(2)}$ and $q = 2$. When $\alpha > \tan^{-1}(l_2/l_3)$, the cohesive crack intersects $\boldsymbol{X}_{\mathrm{R}}^{(3)}$ and $q = 3$. A generalized equation for the deformation gradient tensor decomposition can then be written:

$$\boldsymbol{F}^{(q)}l_q = \boldsymbol{F}_{\mathrm{B}}{}^{(q)}l_q + \boldsymbol{R}_{\mathrm{cr}}\boldsymbol{\delta} \tag{11}$$

where $\boldsymbol{F}^{(q)}$ is the q-th column of $\boldsymbol{F}$, $\boldsymbol{F}_{\mathrm{B}}{}^{(q)}$ is the q-th column of $\boldsymbol{F}_{\mathrm{B}}$, and l_q is the length of the q-th column of $\boldsymbol{X}_{\mathrm{R}}$. Using equation (11) with any $\boldsymbol{F}$ provided by the finite element solver, the cohesive displacement-jump vector $\boldsymbol{\delta}$ can be solved for in terms of $\boldsymbol{F}_{\mathrm{B}}{}^{(q)}$.

2.3 Equilibrium between the Bulk Material and Cohesive Crack

The sum of the bulk material deformation and the cohesive displacement-jump is shown in equation (11) to be equal to the deformation described by the deformation gradient tensor. However, it remains necessary to ensure that the tractions resulting from the deformations of the bulk material and cohesive crack are in equilibrium. In the present method, equilibrium is enforced on the cohesive crack plane with the normal $\hat{\boldsymbol{e}}_{\mathrm{N}}$. The solution for the current bulk deformation gradient is found by minimizing the difference between the cohesive stress vector $\boldsymbol{\tau}$ and the bulk material stress $\boldsymbol{\sigma}_{\mathrm{B}}$ projected onto the cohesive crack.

The cohesive stress vector $\boldsymbol{\tau}$ is determined using the cohesive damage model of González et al. [15] is used. The cohesive stress vector $\boldsymbol{\tau}$ is defined as:

$$\boldsymbol{\tau} = \begin{bmatrix} k_{\mathrm{F}}(1-d_m)\delta_{\mathrm{F}} \\ k_{\mathrm{N}}(1-d_m)\delta_{\mathrm{N}} - k_{\mathrm{N}}d_m\langle-\delta_{\mathrm{N}}\rangle \\ k_{\mathrm{T}}(1-d_m)\delta_{\mathrm{T}} \end{bmatrix} \tag{12}$$

where δ_{N} is the opening displacement-jump, and δ_{F} and δ_{T} are the shear displacement-jumps along the fiber and transverse directions, respectively; k_{F}, k_{N}, and k_{T} are the cohesive penalty stiffnesses in the fiber, crack-normal, and transverse directions, respectively; d_m is the scalar cohesive damage variable; and the operator $\langle x\rangle$ is defined as $\langle x\rangle = (x + |x|)/2$.

The bulk material stress is determined from the bulk material deformation gradient tensor $\boldsymbol{F}_{\mathrm{B}}$ using standard finite stress and strain definitions and Hooke's Law:

$$\boldsymbol{E} = \left(\boldsymbol{F}_{\mathrm{B}}^{\mathrm{T}}\,\boldsymbol{F}_{\mathrm{B}} - \boldsymbol{I}\right)/2 \tag{13}$$

$$\boldsymbol{S} = \boldsymbol{C^d}\!:\boldsymbol{E} \tag{14}$$

where $\boldsymbol{E}$ is the Green-Lagrange strain, $\boldsymbol{S}$ is the 2nd Piola-Kirchhoff stress, and $\boldsymbol{I}$ is the identity tensor. Tensile fiber failure initiation is predicted using an uncoupled maximum strain failure criterion with the fiber-direction Green-Lagrange strain. Fiber damage is represented using the CDM approach of Maimí et al. [2]. Cauchy's stress theorem is used to find the corresponding stress vector $\boldsymbol{t}$ acting on the cohesive interface:

$$\boldsymbol{t} = \boldsymbol{\sigma}_{\mathrm{B}} \cdot \hat{\boldsymbol{e}}_{\mathrm{N}} \tag{15}$$

where $\boldsymbol{\sigma}_{\mathrm{B}}$ is the bulk material Cauchy stress in the reference coordinate system, determined using:

$$\boldsymbol{\sigma}_{\mathrm{B}} = \boldsymbol{F}_{\mathrm{B}}\,\boldsymbol{S}\,\boldsymbol{F}_{\mathrm{B}}^{\mathrm{T}}|\boldsymbol{F}_{\mathrm{B}}|^{-1} \tag{16}$$

To solve for the stress state at equilibrium, a residual stress vector $\boldsymbol{\sigma}_{\mathrm{Res}}$ can be defined in terms of the components of the stress vectors in equations (12) and (15) in the current crack coordinate system:

$$\boldsymbol{\sigma}_{\mathrm{Res}} = \begin{bmatrix} k_{\mathrm{F}}(1-d_m)\delta_{\mathrm{F}} - \boldsymbol{t}\cdot\hat{\boldsymbol{e}}_{\mathrm{F}} \\ k_{\mathrm{N}}(1-d_m)\delta_{\mathrm{N}} - k_{\mathrm{N}}d_m\langle-\delta_{\mathrm{N}}\rangle - \boldsymbol{t}\cdot\hat{\boldsymbol{e}}_{\mathrm{N}} \\ k_{\mathrm{T}}(1-d_m)\delta_{\mathrm{T}} - \boldsymbol{t}\cdot\hat{\boldsymbol{e}}_{\mathrm{T}} \end{bmatrix} \tag{17}$$

Because $\boldsymbol{F}$ is known and $\boldsymbol{\delta}$ is a function of $\boldsymbol{F}$ and $\boldsymbol{F}_{\mathrm{B}}$, the three components of ${\boldsymbol{F}_{\mathrm{B}}}^{(q)}$ are used as the unknown variables that must be found in order to minimize the residual. The multivariate Newton-Raphson method is used to find a converged solution for ${\boldsymbol{F}_{\mathrm{B}}}^{(q)}$:

$${\boldsymbol{F}_{\mathrm{B,new}}}^{(q)} = {\boldsymbol{F}_{\mathrm{B}}}^{(q)} - \left(\frac{\partial\boldsymbol{\sigma}_{\mathrm{Res}}}{\partial{\boldsymbol{F}_{\mathrm{B}}}^{(q)}}\right)^{-1}\boldsymbol{\sigma}_{\mathrm{Res}} \tag{18}$$

A solution is sought until the norm of $\boldsymbol{\sigma}_{\mathrm{Res}}$ is less than a user-defined tolerance value, set by default to 0.01% of the mode I cohesive strength. After a converged solution is found, the cohesive damage model is evaluated for the current $\boldsymbol{\delta}$. If the cohesive damage variable d_m is predicted to increase, a new converged deformation state is sought for the updated d_m using equation (18). If d_m is not predicted to increase, a solution for the current material state has been found, and the results are reported to the FE solver.

3 CASE STUDIES

Two case studies are presented to demonstrate the performance of the DGD method for geometrically nonlinear problems involving large shear deformations. The first case is a single element subjected to simple shear deformation. The second case is a unidirectional open-hole tension (OHT) specimen based on a previous experimental and analytical investigation by Iarve et al. [16]. For both cases, FE models were developed and solved using Abaqus/Explicit 6.13-1 under quasi-static loading conditions with geometric nonlinearity considered [6].

To demonstrate the advantages of incorporating DGD into current CDM modeling approaches, the two case study models were solved using: (*i*) the presented DGD CDM method, and (*ii*) an implementation of the smeared-crack model of Camanho et al. [5] to represent the predictions of a strain-based CDM method. Additional strain-based CDM methods were evaluated, and similar results were found for all strain-based CDM methods evaluated for the two case study models. Predictions obtained using the two material models are evaluated and compared in terms of how the local stresses are affected by predicted matrix cracks and in terms of the details of the predicted overall failure processes.

3.1 Single Element Simple Shear

A single three-dimensional element is deformed in simple shear in the x_1–x_2 plane. The element measures 0.1 mm on each side and is composed of IM7/8552 carbon/epoxy material. The 0° fiber

direction is aligned with the x_1-direction. The relevant material properties for IM7/8552 are provided in Table 1. An eight-node C3D8R solid element with reduced integration is used. The four nodes on the surface at $x_2 = 0$ mm are constrained in the x_1- and x_2-directions. The four nodes on the surface at $x_2 = 0.1$ mm are constrained in the x_2-direction and displaced 0.05 mm in the positive x_1-direction. The four nodes on the surface at $x_3 = 0$ mm are constrained in the x_3-direction.

Property	Description	Value		Ref.
E_1	Young's modulus, fiber-direction	171,420	MPa	[17]
E_2	Young's modulus, matrix-direction	9,080	MPa	[17]
G_{12}	Shear modulus	5,290	MPa	[17]
ν_{12}	Poisson ratio, 1–2	0.32	–	[17]
ν_{23}	Poisson ratio, 2–3	0.52	–	[5]
Y_T	Mode I matrix strength	62.3	MPa	[17]
S_L	Mode II matrix strength	92.3	MPa	[17]
X_{fT}	Fiber tensile strength	2,326	MPa	[17]
G_{Ic}	Mode I matrix fracture toughness	0.277	kJ/m^2	[17]
G_{IIc}	Mode II matrix fracture toughness	0.788	kJ/m^2	[17]
η	Benzeggagh-Kenane coefficient	1.634	–	[5]
G_{fT}	Fiber tensile fracture toughness	134.	kJ/m^2	[18]

Table 1: IM7/8552 material properties.

The expected response to simple shear deformation is an initially linear-elastic response leading up to the formation of a matrix crack (i.e., $d_m > 0$) with a crack normal in the x_2-direction, followed by mode II dominant linear softening until the crack is fully formed (i.e., $d_m = 1$). After $d_m = 1$, all stress components should be equal to zero, as any further simple shear deformation should then represent the sliding of two separated, undeformed volumes of material.

The model using the DGD CDM method predicts a nearly perfect mode II response to simple shear deformation, as is evident by the shear stress-displacement results shown in Figure 3. Even at large shear displacements, no load transfer across the crack is observed. The model with the strain-based CDM method accurately predicts the initiation of matrix damage and the initial rate of energy dissipation, as expected. With increasingly large shear deformation, however, increasingly large load transfer across the matrix crack is observed.

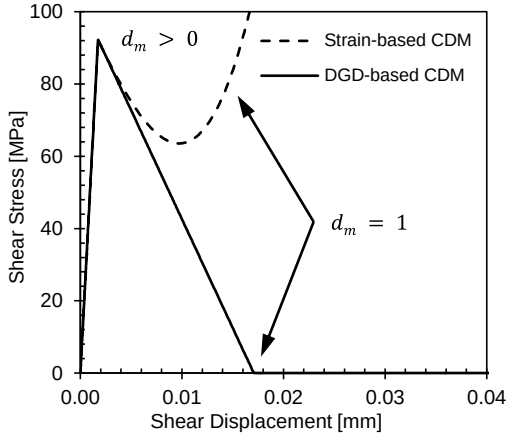

Figure 3: Shear stress-displacement FE results for the single element simple shear model. Shear stress is calculated as the sum of the x_1-direction nodal forces of the nodes on the $+x_2$-direction surface of the element, divided by 0.01 mm^2. [12]

The use of incorrectly defined coordinate systems for the crack and the bulk material can also lead to the prediction of spurious, secondary failure modes. For instance, the simple shear model with the strain-based CDM method predicts increasing compressive fiber stresses with increasing simple shear deformation after the formation of the matrix crack. With increasing shear deformation, these nonphysical compressive fiber stresses in the model with the strain-based CDM method eventually satisfy the compressive fiber failure criterion, causing spurious fiber damage initiation (not shown in Figure 3).

3.2 Unidirectional Open-Hole Tension

A model of a unidirectional [0_8] open-hole tension specimen is shown in Figure 4. The specimen has a length l equal to 50.8 mm, a width w equal to 12.7 mm, and a thickness t equal to 1.0 mm. The specimen contains a hole at its center with a diameter d equal to 3.175 mm. The fiber-direction is aligned with the specimen length. The nodes on the surface at $x_1 = 0$ are constrained in the x_1-direction. The nodes along the edge at $x_1 = 0$ and $x_2 = 0$ and the edge at $x_1 = l$ and $x_2 = 0$ are constrained in the x_2-direction. The nodes on the surfaces at $x_1 = 0$ and $x_1 = l$ are constrained in the x_3-direction. Load is introduced by uniformly displacing the nodes on the surface at $x_1 = l$ in the positive x_1-direction.

Three-dimensional, eight-node C3D8R solid elements with reduced integration are used throughout the model. A fiber-aligned mesh is used to avoid shear stress transfer due to element shear locking, based on the recommendations of Song et al. [19] for similar laminated OHT models. All of the elements along the expected matrix splitting path are cuboids and have an element length equal to 0.127 mm in the x_2-direction. Four layers of elements of equal thickness are used through the thickness of the laminate.

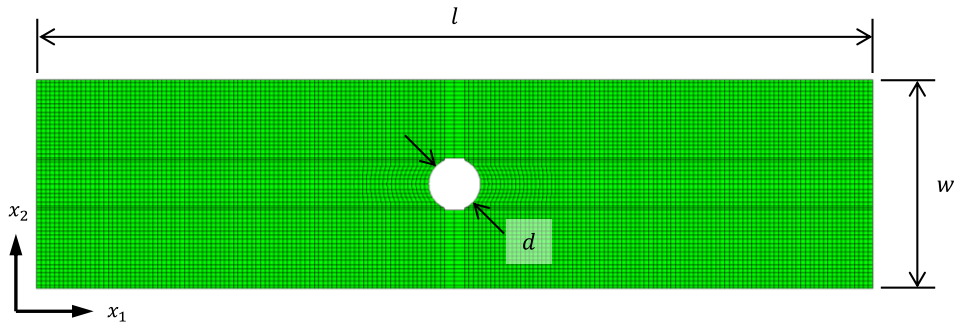

Figure 4: Mesh and geometry for the unidirectional OHT FE model. [12]

Based on the experimental work of Iarve et al. presented in reference [15], the expected failure process for the unidirectional OHT specimen is as follows: (*i*) matrix splitting cracks form tangent to the hole and extend along the x_1-direction toward the model edges; (*ii*) as the matrix cracks extend, the fiber stress concentration at the hole diminishes until a uniform σ_{11} stress state is established in the remaining ligaments on either side of the hole; (*iii*) the specimen fails when σ_{11} in the ligaments reaches X_{fT} at a load of approximately:

$$22.2 \text{ kN} = X_{fT} \times (w - d) \times t \tag{19}$$

Because no compressive matrix or fiber damage should occur in the model, and to better isolate the effects of defining the material stress state via the DGD method, the compressive matrix and fiber strength and fracture toughness properties for the strain-based CDM model were artificially increased to avoid their activation in the unidirectional OHT model.

Analysis predictions obtained with the model using the DGD CDM method are shown by the black curve in Figure 5, and the predictions are as expected. Matrix damage initiation occurs at four locations that are tangent to the hole at an applied tensile load of 2.4 kN. At a tensile load of 4.2 kN, the four

matrix splitting cracks rapidly extend along the length of the specimen to an average length of 17 mm. Cracks of this length reduce the stiffness of the specimen, as can be seen in Figure 5 with a shift in the curve. The matrix splitting cracks then propagate slowly toward the model edges with continued loading. A peak load of 22.3 kN is reached just prior to tensile fiber failure originating at the edge of the hole in the intact ligaments. The extent of predicted matrix damage is shown by the red elements just prior to failure in Figure 6a.

The OHT model with the strain-based CDM method predicts matrix crack initiation and the initial growth of the matrix cracks at loads that are in close agreement with the DGD model predictions. However, when the cracked elements undergo large shear deformation, load transfer across the cracked elements occurs and further matrix crack growth is slowed. The slower rate of matrix splitting crack growth predicted by the strain-based CDM model is apparent in the slower rate of change in the slope of the load-displacement response, as shown by the gray curve in Figure 5. Load transfer across the first set of four matrix splitting cracks causes secondary and tertiary rows of matrix cracks to develop, as shown in in Figure 6b. Regions of the mesh where multiple adjacent matrix cracks develop (i.e., rows of softened elements without any intact elements remaining between them) undergo severe distortion. The distortion of the mesh leads to premature failure of the model at a load of 9.6 kN.

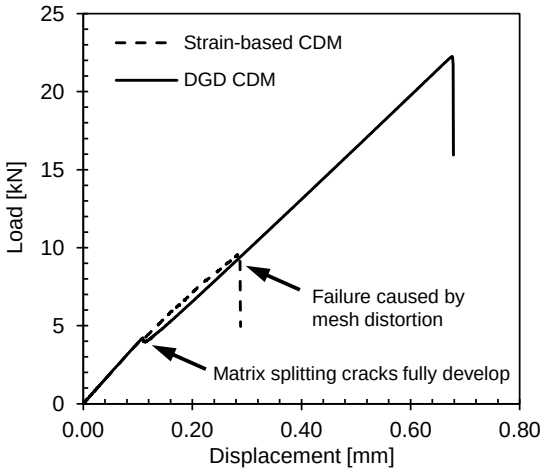

Figure 5: Load-displacement results of the unidirectional OHT models. [12]

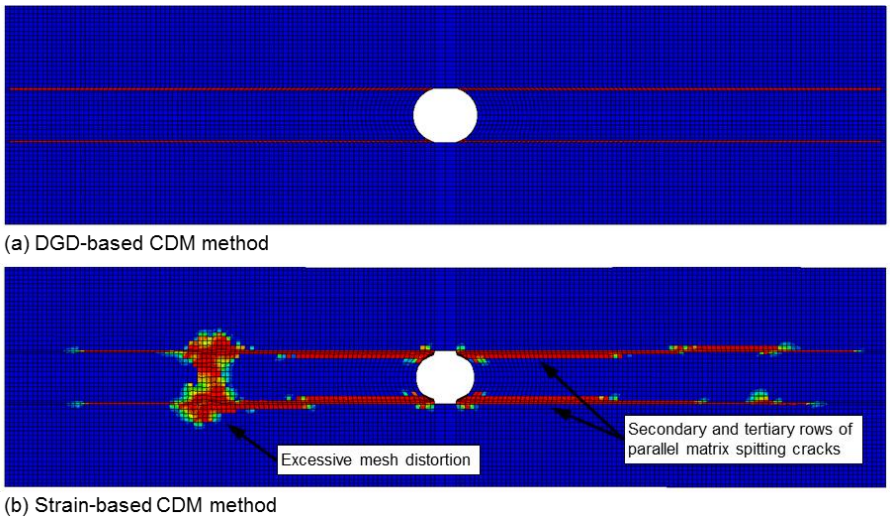

Figure 6: Predicted matrix damage state at peak load for the unidirectional OHT models. Blue represents intact material and red represents a fully developed matrix crack. [12]

Iarve et al. [15] and Song et al. [19] demonstrated that CDM modeling approaches are unable to eliminate the stress concentration at the hole that should follow the formation of the splitting cracks and the present results confirm those observations. Stress concentration factors equal to approximately 1.5 are predicted by the model with the strain-based CDM method after the formation of the matrix splitting cracks, as shown in Figure 7a. The analysis conducted with the DGD CDM method predicts a more uniform σ_{11} distribution after the extension of the matrix splitting cracks, as shown in Figure 7b.

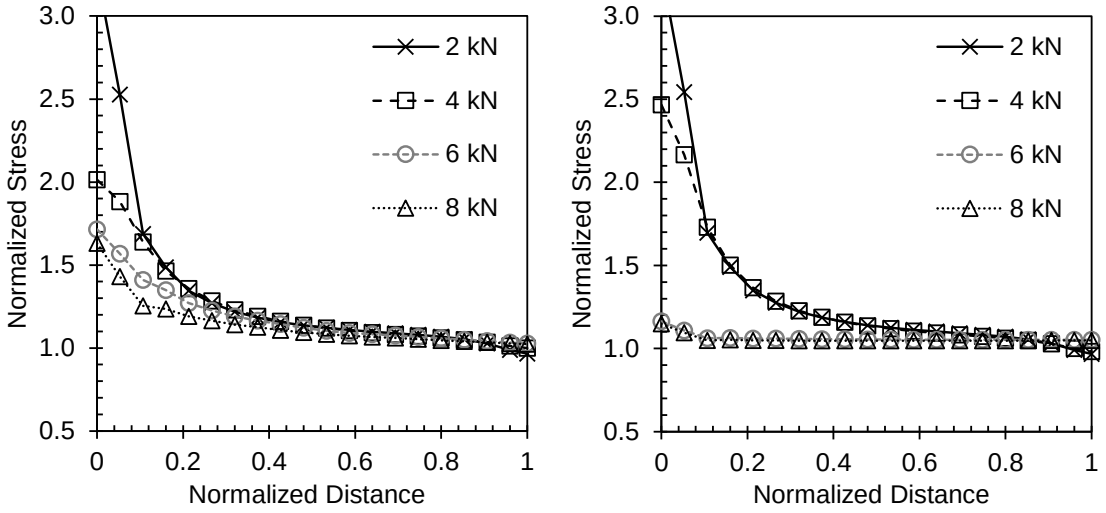

Figure 7: Normalized fiber-direction stress versus normalized distance from the hole along the mid-section of the unidirectional OHT model. The fiber-direction stress is normalized by $E_1\Delta/L$, where Δ is the applied x_1-direction displacement and L is the specimen length.

4 CONCLUSIONS

A method is presented which improves the predictive capability of continuum damage mechanics (CDM) methods for fiber-reinforced materials in geometrically nonlinear finite element models. The method involves the additive decomposition of the deformation gradient tensor into 'crack' and 'bulk material' components and determining the current crack opening displacement by assuming stress equivalence on the crack plane. The presented approach allows for accurate representation of crack kinematics in CDM progressive damage analyses. The implementation of the presented method as a constitutive material model allows for the method to be applied to existing two- or three-dimensional solid or shell finite elements. The potential improvements to the accuracy of progressive damage finite element models have been demonstrated for a single element subjected to simple shear deformation and for a tension-loaded unidirectional open-hole specimen model. In both cases, the presented method performs better than existing approaches in terms of reducing the transfer of load across open matrix cracks and avoiding the prediction of spurious secondary failure modes when subjected to large shear deformations.

REFERENCES

[1] Matzenmiller A, Lubliner J, Tayler RL. A constitutive model for anisotropic damage in fiber-composites. *Mechanics of Materials* 1995; **20**:125–52.

[2] Maimí P, Camanho PP, Mayugo JA, Dávila CG. A continuum damage model for composite laminates: Part I – Constitutive model. *Mechanics of Materials* 2007; **39**:897–908.

[3] Lapcyzyk I, Hurtado JA. Progressive damage modeling in fiber-reinforced materials. *Composites Part A: Applied Science and Manufacturing* 2007; **38**:2333–41.

[4] Van Der Meer FP, Sluys LJ. Continuum models for the analysis of progressive failure in composite laminates. *Journal of Composite Materials* 2009; **43**(20):2131–56.
[5] Camanho PP, Bessa MA, Catalanotti G, Vogler M, Rolfes R. Modeling the inelastic deformation and fracture of polymer composites – Part II: Smeared crack model. *Mechanics of Materials* 2013; **59**:36–49.
[6] ABAQUS (2013). Abaqus 6.13 Online Documentation. Dassault Systèmes, Providence, RI, USA.
[7] Prabhakar P, Waas AM. A novel continuum-decohesive finite element for modeling in-plane fracture in fiber reinforced composites. *Composites Science and Technology* 2013; **83**:1–10.
[8] Ling D, Yang Q, Cox B. An augmented finite element method for modeling arbitrary discontinuities in composite materials. *International Journal of Fracture* 2009; **156**:53–73.
[9] Iarve EV, Gurvich MR, Mollenhauer DH, Rose CA, Dávila CG. Mesh-independent matrix cracking and delamination modeling in laminated composites. *International Journal for Numerical Methods in Engineering* 2011; **88**(8):749–73.
[10] Chen BY, Pinho ST, De Carvalho NV, Baiz PM, Tay TE. A floating node method for the modeling of discontinuities in composites. Engineering Fracture Mechanics 2014; **127**:104–34.
[11] Rose CA, Dávila CG, Leone FA. Analysis methods for progressive damage of composite structures. NASA/TM–2013-218024.
[12] Leone FA. Deformation gradient tensor decomposition for representing matrix cracks in fiber-reinforced materials. *Composites Part A: Applied Science and Manufacturing* (submitted).
[13] Pinho ST, Dávila CG, Camanho PP, Iannucci L, Robinson P. Failure models and criteria for FRP under in-plane or three-dimensional stress states including shear nonlinearity. NASA/TM–2005-213530.
[14] Catalanotti G, Camanho PP, Marques AT. Three-dimensional failure criteria for fiber-reinforced laminates. *Composite Structures* 2013; **95**:63–79.
[15] González EV, Maimí P, Turon A, Camanho PP, Renart J. Simulation of delamination by means of cohesive elements using an explicit finite element code. *Computers, Materials and Continua* 2009; **9**(1):51–92.
[16] Iarve EV, Mollenhauer D, Kim R. Theoretical and experimental investigation of stress redistribution in open hole composite laminates due to damage accumulation. *Composites Part A: Applied Science and Manufacturing* 2005; **36**(2):163–71.
[17] Camanho PP, Maimí P, Dávila CG. Prediction of size effects in notched laminates using continuum damage mechanics. *Composites Science and Technology* 2007; **67**:2715–27.
[18] Catalanotti G, Camanho PP, Xavier J, Dávila CG, Marques AT. Measurement of resistance curves in the longitudinal failure of composites using digital image correlation. *Composites Science and Technology* 2010; **70**:1986–93.
[19] Song K, Li Y, Rose CA. Continuum damage mechanics models for the analysis of progressive failure in open-hole tension laminates. *52nd AIAA/ASME/ASCE/AHS/ASC Structures, Structural Dynamics and Materials Conference*. 4–7 April 2011. Denver, Colorado.